Journal of Materials Chemistry A

Accepted Manuscript

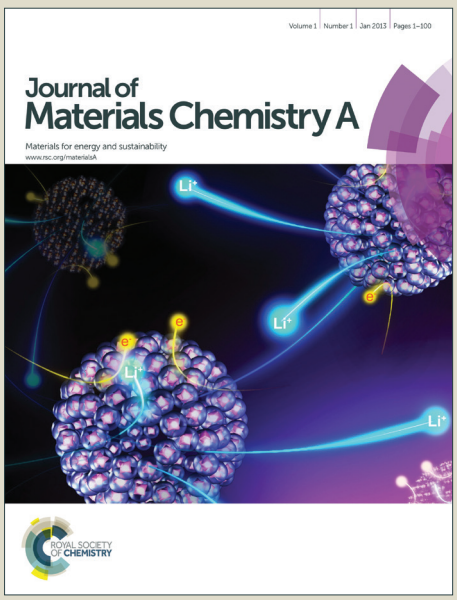

ROYAL SOCIETY OF CHEMISTRY

www.rsc.org/materialsA

Journal Name

ARTICLE

Carbon Microtube/Graphene Hybrid Structure for Thermal Management Application

Received 00th January 20xx,
Accepted 00th January 20xx

DOI: 10.1039/x0xx00000x

www.rsc.org/

Hui Bi,[a] Haining Huang,[a] Feng Xu,[a] Tianquan Lin,[a] Hui Zhang,[a]* and Fuqiang Huang[a,b]*

Carbon microtube/graphene (CMT/GR) hybrid structure has been prepared from nature biomass material (absorbent cotton) by the carbonization and continuous chemical vapor deposition (CVD) of graphene at 1200 °C, and the CVD graphene nanosheets with few-layer structure are uniformly coated on the CMTs' surface. The CMT/GR composite has a hollow tubular structure, and exhibits a specific surface area of ~312 m^2 g^{-1} and highly hydrophobic characteristic (contact angle: ~128°). The CMT/GR acts as a thermal conductive supporting framework, and organic octadecanoic acid (OA) is easily impregnated into the CMT/GR by capillary force. The CMT/GR/OA composite has a thermal conductivity of ~0.69 W m^{-1} K^{-1} at a CMT/GR loading fraction of approx. 10 wt.%, which is about 4.3 times larger than that of the OA (~0.16 W m^{-1} K^{-1}). The CMT/GR/OA composite presents a high heat storage capacity of ~174 J g^{-1}, very close to the value of the OA (~186 J g^{-1}), and shows a good thermal reliability even after 500 melting/freezing cycles. The present research provides a novel shape-stabilized PCM for thermal energy storage as well as some new insights into the design of preparing the CMT/GR hybrid structure from nature resource.

Introduction

With energy supplies intense increasingly and energy utilization being concerned on particularly, phase change materials (PCMs) have are widely used for thermal energy storage and temperature control in thermal insulation, solar heating system and electric device,[1-3] due to their high thermal storage capacity and narrow temperature range.[4-6] However, the lack of segregation, chemical stability and poor thermal conductivity are main bottlenecks of the PCMs to date.[7,8] Thus, a supporting framework with highly thermal conductivity is necessary for the heat transport in thermal energy storage system to not only increase the heat transport ability of the PCMs, but also prevent the seepage of the molten PCMs.[9-11] In the past few decades, various supporting materials (metal foams,[12] porous ceramics,[13] graphene/ceramic composites,[14-16] *etc*.) have been used to remedy undesirable properties of the PCMs to enhance their thermal conductivities. However, these supporting materials significantly increase the weight and/or cost to thermal storage system, and/or some of them are incompatible with the PCMs.

Graphene, a new two dimensional allotrope of carbon, is more promising as the filler than carbon nanotubes, graphite, carbon black, *etc.*, due to its better thermal coupling to the PCM materials.[17-19] Therefore, graphene has exhibited great potential applications in thermal management and energy storage devices because of its unique physical properties.[20] For instance, the thermal conductivity of graphene reaches up to 1000-3000 W m^{-1} K^{-1},[21-25] ten times greater than copper. Graphene possesses a large specific surface area of ~3100 m^2 g^{-1},[26] which can offer plenty of interfaces with the PCMs to reduce the thermal contact resistance. Additionally, graphene also shows the hydrophobic nature (contact angle with water: ~90°) to be compatible with the PCMs (such as organic stearic acid, paraffin wax, *etc*.).[27] However, the above advantages are strongly dependent on the crystalline quality of graphene. Among many approaches of graphene preparation, chemical vapor deposition (CVD) method is considered as one of the most promising techniques to achieve the large scale preparation of high quality graphene. Therefore, it is reasonable to consider that the CVD graphene can be used as a thermal conductive supporting framework to enhance the thermal transport properties of the PCMs.

In this work, we have fabricated low-cost, hollow carbon microtube/graphene (CMT/GR) hybrid structure from nature resource (absorbent cotton) by the carbonization and CVD method for thermal management application. The CMT/GR possesses low density, large specific surface area, highly hydrophobic characteristic and suitable thermal conductivity, and can act as a supporting framework to apply in PCMs. After the graphene growth on the CMTs' surface, the graphene nanosheets can greatly decrease thermal contact resistance with octadecanoic acid (OA), and high thermal conductivity of ligaments in the CMT/GR significantly improve the thermal

[a]*CAS Key Laboratory of Materials for Energy Conversion, Shanghai Institute of Ceramics, Chinese Academy of Sciences, Shanghai 200050, P.R. China*
[b]*Beijing National Laboratory for Molecular Sciences and State Key Laboratory of Rare Earth Materials Chemistry and Applications, College of Chemistry and Molecular Engineering, Peking University, Beijing 100871, P.R. China*
†Electronic Supplementary Information (ESI) available: [details of any supplementary information available should be included here]. See DOI: 10.1039/x0xx00000x

transport property of the CMT/GR/OA composite (~0.69 W m^{-1} K^{-1}). Moreover, the latent heat of the CMT/GR/OA composite (~10 wt.% loading of the CMT/GR as the supporting framework) reaches up to 174 J g^{-1}, and changes little after 500 thermal cycles, which is very close to the OA value (~186 J g^{-1}).

Experimental

Preparation for the CMT/GR and CMT/GR/OA composites

The absorbent cotton was pressed into φ 26 mm disks under 10 MPa for 2 min. The carbonization process was carried out to prepare CMTs with a gas flow of H_2: Ar =50: 300 sccm for 120 min at 1200 °C. After the carbonization, a small amount of CH_4 (~5 sccm) was introduced into the Al_2O_3 tube at 1200 °C for 60 min to continuously grow graphene on the CMTs' surface for the fabrication of the CMT/GR hybrid structure. Then, the CMT/GR structure was directly placed into the melted OA at 80 °C for 4 h to obtain the CMT/GR/OA composite. The composite was cooled down to the room temperature, and further polished by sand paper to obtain a disc with the diameter of 12.7 mm and thickness of 2 mm for thermal conductivity and thermal imager measurements.

2.2 Characteristics and measurement

The CMT/GR morphology was observed by a Hitachi S-4800 field emission scanning electron microscope (FESEM). High resolution transmission electron microscope (HRTEM) images were obtained by JEOL 2100F. Raman spectra were collected on a thermal dispersive spectrometer using a laser with an excitation wavelength of 532 nm at a laser power of 8 mW. X-ray photoelectron spectroscopy (XPS) analysis (Thermo VG Scientific) was undertaken under high vacuum using Al-Ka 1486.6 eV radiation at 400 W (15 kV). Nitrogen adsorption measurements were performed with ASAP 2020M (Micromeritics) to obtain the specific surface area and pore size distribution. Water contact angles were measured with a Data-Physics OCA 20 (Germany). A thermal imager (SC305, Flir system USA) was used to record temperature distribution images of the PCMs, and its spatial resolution and temperature resolution of the instrument is 1.36 mrad and 0.1 ℃, respectively. The DSC curve was measured by the Q100 Thermal Analyser. The in-plane thermal conductivity was measured using LFA 447 laser conductometer at the temperatures of 20 °C-80 ℃, and standard sample is Pyrex 7740 glass.

Results and discussion

The preparation process of the CMT/GR/OA composite is shown in Figure 1a. Firstly, the absorbent cotton was pressed into a disc (Figure 1b), then acted as the precursor to further carbonize for the formation of CMTs at 1200 °C. After the carbonization, carbon resource CH_4 was introduced to directly grow highly thermal conductive graphene nanosheets coated on the CMTs' surface. The CMT/GR hybrid structure was used as a highly thermal conductive supporting framework to increase the thermal transport property of the OA PCM (Figure 1c-d). Additionally, the graphene nanosheets coated the CMTs are also good compatible with the OA, which effectively stabilize the OA in shape.

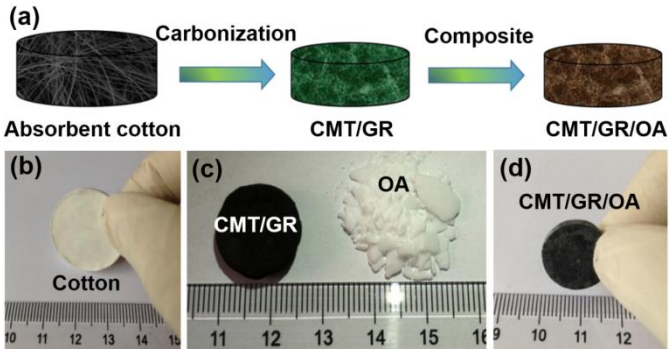

Figure 1. (a) Preparation process of the CMT/GR/OA composite. (b-d) Digital images of the absorbent cotton, CMT/GR and CMT/GR/OA composites.

Compared with the absorbent cotton, the CMT/GR hybrid structure shows some shrink in size, and the content of graphene in the CMT/GR is approx. 9.2 wt.%. During the carbonization, the weight loss of the absorbent cotton precursor is about 85 wt.%, which mainly comes from the dehydration, decarbonylation and decarboxylation of the precursor. The CMT/GR hybrid structure still keeps excellent structural integrity (Figure 1c), which is important for the further thermal management application. The morphology and microstructure of the CMT/GR were characterized by FESEM and HRTEM, as shown in Figure 2. The CMT/GR composite exhibits hollow micro-tubular structure, and has the diameter and wall thickness of 1-10 μm and several hundreds of nanometers, respectively (Figure 2a & 2b). From the FESEM image of the CMT/GR (Figure 2c & 2d), a large amount of the vertical or tilted graphene nanosheets uniformly grow along the inside and outside surfaces of the CMT. The HRTEM images of the CMT/GR show clearly that the graphene nanosheets are coated tightly on the CMTs' surface (Figure 2e), and the graphene nanosheets have few-layer structure (Figure 2f).

Raman spectroscope was used to investigate the CMT/GR microstructure, as shown in Figure 3a. The Raman spectrum for the CMTs displays two obvious peaks at around 1368 cm^{-1} (D band) and 1591 cm^{-1} (G band), attributed to defected carbon crystallite and crystalline graphite, respectively. The ratio of intensity of D band to G band is approx. 1.3, indicating the poor graphitic structure of the CMTs. After the CVD growth of graphene, the Raman spectrum shows an additional peak (2D band) at ~2683 cm^{-1}, and the ratio of 2D band to G band is about 0.82. The Raman features further confirm the presence of graphene nanosheets with few-layer structure coated on the CMTs' surface,[28,29] consistent with the FESEM and HRTEM results (Figure 2). Moreover, the ratio of D band to G band of CMT/GR is about 1.1, significantly lower than that of CMTs (~1.3), showing relatively good crystalline quality of CVD graphene nanosheets,[30] compared with the CMTs.

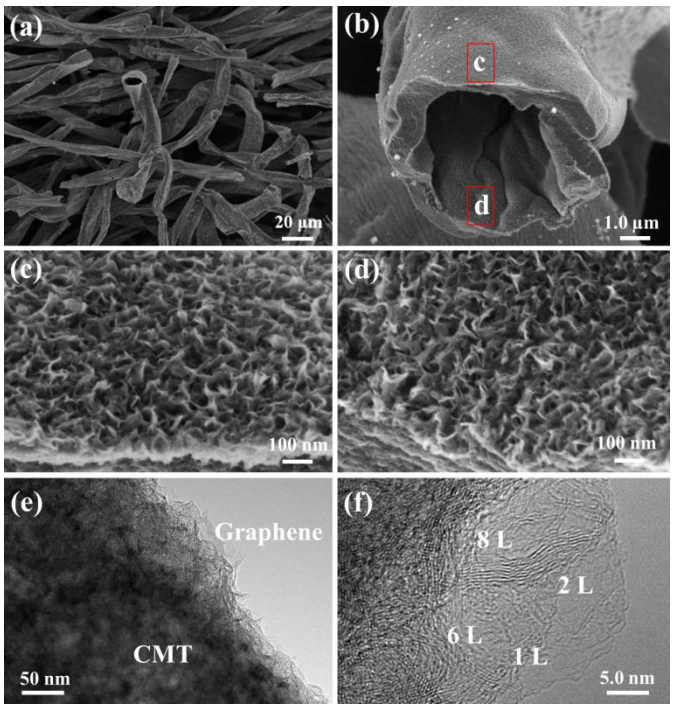

Figure 2. (a) FESEM image of the CMT/GR on the whole. (b) SEM image of an individual hollow CMT/GR. (c, d) FESEM images of graphene nanosheets grown on (c) outside and (d) inside surfaces of the CMT. (e) TEM image of edge of the CMT/GR. (f) HRTEM image of graphene nanosheets on the CMT surface.

XPS analyses were performed to investigate the chemical state and element composition of the CMT/GR. XPS spectrum (Figure 3b) shows the weight percentage of non-oxygenated carbon in the CMT/GR hybrid structure is estimated to be 99.4 at.%. High resolution XPS spectrum of C 1s peak of the CMT/GR is obtained (inset of Figure 3b), and the C 1s peak can be fitted with four different peaks: a highly intensive peak associated with the binding energy (~284.7 eV) of sp^2 hybridised carbon atoms and three weak peaks at ~285.2 eV, ~287.1 eV and ~288.8 eV, which are associated with the sp^3 hybridised C–O, C=O and O-C=O, respectively.[31]

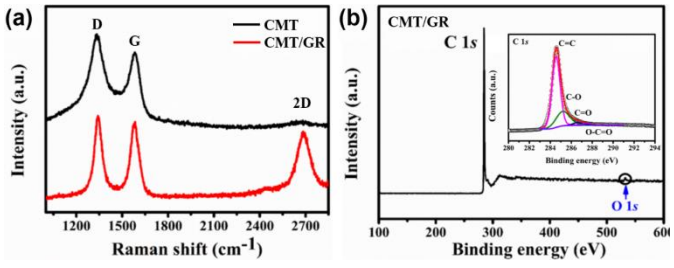

Figure 3. (a) Raman spectra of the CMT and CMT/GR. (b) XPS spectrum of the chemical composition of the CMT/GR, and the inset showing the XPS spectrum of C 1s peak of the CMT/GR.

Isothermal curve of nitrogen adsorption shows the trend of slow filling in adsorption in the entire pressure range and the rapid desorption in the middle pressure (Figure 4a), suggesting a typical ink-bottle-like pore structure of the CMT/GR.[32-34] The CMT/GR composite has a large specific surface area of ~312 $m^2 g^{-1}$ and a large amount of porous structure formed by the evaporation of H_2O and CO_2 in the carbonization process at 1200 °C.[35] The average pore size of the supporting framework is critical for the performance of the PCMs. Small pores (micropore: < 2 nm) generally obstruct the molecular motion of organic PCMs, whereas large pores (macropore: > 50 nm) weaken the capillary force, leading to the seepage of the molten PCMs.[11,36,37] The pore size distribution of the CMT/GR is mainly from 2.0 nm and 20 nm, belonging to mesopore structure (inset of Figure 4a). Thus, the large specific surface area and plenty of mesopores can make the CMT/GR use as a supporting framework for the preparation of the PCMs.

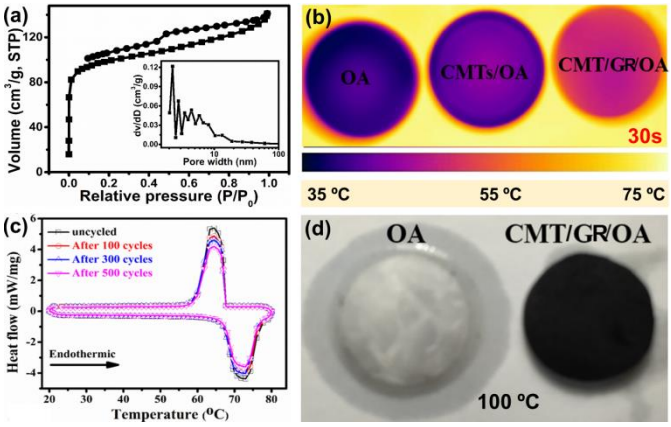

Figure 4. (a) Pore size distribution of the CMTs and CMT/GR, and the inset showing isothermal curve in nitrogen adsorption. (b) Thermal transport evolution of the OA, CMT/OA and CMT/GR/OA composites. (c) DSC thermograms of the CMT/GR/OA composite before and after thermal cycling. (d) Absorption performance comparison of the OA and CMT/GR on 100 °C heating plate.

Graphene growth on CMTs follows the nucleation and growth mechanism. At 1200 °C, carbon resource (CH_4) was directly decomposed into various carbon radicals/species. The primary carbon species were further captured by large amounts of structural defects (active sites) of the CMTs to randomly form graphene nucleation centers on the CMT surface. As the growth proceeded, the graphene islands grew larger and larger, and got connected with neighbouring nanosheets to eventually form a continuous graphene network structure (Figure 2). The growth process is similar to graphene growth on the insulating substrates (Al_2O_3, SiO_2, *etc.*),[15,30] but the growth of graphene on the CMT surface is much faster than the insulating substrates. Because that the structural defects of the CMTs can supply a much more nucleation centers to significantly promote the graphene growth.

To investigate the heat transport property after the introduction of CMT/GR into OA, we recorded the temperature distribution images of the OA, CMT/OA and CMT/GR/OA composites by a thermal imager. A video was taken using the thermal imager to record the thermal

evolution of the samples. When all the samples were put on the heating plate, the samples started to heat up, and the heating rates depend on their thermal transport properties. Figure 4b shows that the temperature increase of the CMT/GR/OA composite is more quickly than the CMT/OA composite and OA at 30s, proving that the CMT/GR hybrid structure greatly enhances the thermal transport property of the OA.

The cross-sectional SEM image (Figure S1a) shows that the CMT/GR has been uniformly dispersed in the OA PCM, and the filler content, density (ρ), thermal diffusivity (α), heat specific capacity (C_p) and thermal conductivity (κ) of the OA, CMTs/OA and CMT/GR/OA composites have been listed in Table 1. The results show that the thermal conductivity of OA is very low, just ~0.16 W m^{-1} K^{-1}, much lower than the requirement of applications. When the CMTs were used as the supporting framework, an up to 1.8-fold increase in thermal conductivity (~0.28 W m^{-1} K^{-1}) can be obtained by adding approx. 10 wt.% CMTs into the OA. Furthermore, after coating graphene nanosheets with few-layer structure on the CMTs' surface, the thermal conductivity of the CMT/GR/OA composite can be greatly improved up to 0.69 W m^{-1} K^{-1}, 2.5 times higher than the value of the CMT/OA composite, even over four times value of the OA. At a very low graphene loading fraction of 0.92 wt.% in the CMT/GR/OA composite, the improvement effect in the thermal conductivity is significantly superior to the expanded graphite, carbon fiber, carbon nanotube and reduced graphene oxide at a similar content,[38-40] indicating that the CVD graphene nanosheets play an important role in enhancing the thermal transport property of the OA PCM.

Table 1. The filler content in the OA PCM, density (ρ), thermal capacity (C_p), thermal diffusivity (α) and thermal conductivity (κ) of the OA, CMT/OA and CMT/GR/OA composites.

Sample	Content wt.%	ρ g cm^{-3}	C_p J g^{-1} K^{-1}	α mm^2 s^{-1}	κ W m^{-1} K^{-1}
OA	0	0.94	1.95	0.086	0.16
CMT/OA	10	0.83	1.81	0.185	0.28
CMT/GR/OA	10	0.85	1.81	0.448	0.69

In order to further investigate the thermal cycle stability of the CMT/GR/OA composite, we also carried out the thermal cycling tests for 500 cycles (Figure 4c). When the temperature is close to the melting point of the OA, the CMT/GR/OA composite undergoes a solid-liquid phase change. Heat is stored during the phase change progress by the latent heat effect, and the CMT/GR/OA composite has a latent heat of ~174 J g^{-1}, which is very close to the value of the OA (~186 J g^{-1}). After 500 cycles, the melting and freezing temperatures of the CMT/GR/OA composite change little, and the latent heat of the CMT/GR/OA composite changes a little (less than 10%). This indicates that the CMT/GR/OA composite exhibits excellent thermal cycle stability, which can be further confirmed by the observation of the CMT/GR well dispersed in the OA PCM after the solid-liquid phase change (Figure S1b). Figure S2 shows thermal conductivities as a function of temperature for the CMT/GR/OA composite, and the temperature range was selected to correspond to the operating temperature of the OA PCM. The thermal conductivities only weakly depend on temperature, decreasing slightly with temperature varying from 20 °C to 80 °C. The weak dependence is an extra benefit for CMT/GR/OA practical applications. Moreover, Figure 4d shows that there is almost no seepage of the CMT/GR/OA composite at 100 °C, whereas the OA alone completely melts, indicating that the CMT/GR supporting framework also effectively stabilizes the OA PCM in shape (Figure 4d).

The thermal transport and cycle stability improvement of the PCM is attributed to the unique structure of the CMT/GR hybrid composite. The CMTs not only provide open pores to be filled with the OA PCM, but also contain interpenetrated conductive pathways as the supporting framework to enhance the thermal conductivity of the OA PCM to some extent. Additionally, graphene nanosheets coated on the CMTs' surface have higher thermal conductivity than the CMTs for the further improvement of the PCM thermal conductivity. More importantly, the CVD graphene nanosheets have relative high crystalline quality, and the CMT/GR composite has a large contact angle (~128°) with water (Figure S3a), which indicates the highly hydrophobic characteristic of the CVD graphene. As shown in Figure S3b, the contact angle with the OA is almost 0° (the CMT/GR hybrid structure), showing the excellent oleophilic property of graphene. The hydrophobic and oleophilic characteristics make the CMT/GR hybrid structure provide the good compatibility with the OA PCM, which is easily impregnated into the CMT/GR composite by capillary force. Therefore, the CMT/GR composite can be not only well dispersed in the OA PCM (Figure S1), and but also effectively stabilize the OA in shape (Figure 4d), even at high temperature. Excellent thermal conductive property and structural stability make the CMT/GR supporting framework for promising thermal transport, energy storage and saving applications in energy storage and conversion devices, such as lithium ion batteries, solar cells, *etc.*[20,41]

Conclusions

In summary, we have fabricated hollow tubular CMTs from nature biomass resource (absorbent cotton) by the carbonization at 1200 °C. After the continuous CVD of graphene on the CMTs' surface, the CMT/GR hybrid structure has a large specific surface area of ~312 m^2 g^{-1} and plenty of mesoporous structure. Based on the highly thermal conductive, oleophilic and hydrophobic characteristics of CMT/GR, the CMT/GR composite can act as the supporting framework to easily composite OA by capillary force for the fabrication of the shape-stabilized PCM. The CMT/GR/OA composite (approx. 10 wt.% CMT/GR in composite) has a high thermal conductivity of ~0.69 W m^{-1} K^{-1}, which is about 4.3 times larger than that of the OA (~0.16 W m^{-1} K^{-1}). The latent heat of the CMT/GR/OA composite is 174 J g^{-1}, which is very close to the value of the OA. Moreover, the CMT/GR/OA composite has an excellent

thermal reliability and chemical stability, even after 500 heating and freezing cycles.

Acknowledgements

H. Bi, H. N. Huang and F. Xu contributed equally to this work. Financial support from the Natural Science Foundation of China (Grants No. 51125006, 91122034, 61376056, 51202274, 51202275 and 51402336) and the Science and Technology Commission of Shanghai (Grant No.14YF1406500).

References

1 A. M. Khudhair and M. M. Farid, *Energy Convers. Manage.*, 2004, **45**, 263.
2 M. Kenisarin and K. Mahkamov, *Renew. Sust. Energy Rev.*, 2007, **11**, 1913.
3 C. V. Hémery, F. Pra, J. F. Robin and P. Marty, *J Power Sources*, 2014, **270**, 349.
4 A. Abhat, *Sol. Energy*, 1983, **30**, 313.
5 M. M. Farid, A. M. Khudhair, S. A. K. Razack and S. Al-Hallaj, *Energy Convers. Manage.*, 2004, **45**, 1597.
6 A. Sharma, V. V. Tyagi, C. R. Chen and D. Buddhi, *Renew. Sust. Energy Rev.*, 2009, **13**, 318.
7 Y. Zhong, M. Zhou, F. Huang, T. Lin and D. Wan, *Sol. Energy Mater. Sol. C*, 2013, **113**, 195.
8 H. N. Huang, H. Bi, M. Zhou, F. Xu, T. Q. Lin, F. Liu, L. Zhang, H. Zhang and F. Q. Huang, *J. Mater. Chem. A*, 2014, **2**, 18215.
9 K. Lafdi, O. Mesalhy and A. Elyafy, *Carbon*, 2008, **46**, 159.
10 A. Sari and A. Karaipekli, *Sol. Energy Mater. Sol. C*, 2009, **93**, 571.
11 A. Elgafy and K. Lafdi, *Carbon*, 2005, **43**, 3067.
12 C. Y. Zhao, W. Lu and Y. Tian, *Sol. Energy*, 2010, **84**, 1402.
13 M. Mehrali, S. T. Latibari, M. Mehrali, H. S. C. Metselaar and M. Silakhori, *Energy Convers. Manage.*, 2013, **67**, 275.
14 M. Zhou, H. Bi, T. Q. Lin, X. J. Lu, F. Q. Huang and J. H. Lin, *J. Mater. Chem. A*, 2014, **2**, 2187.
15 M. Zhou, T. Lin, F. Huang, Y. Zhong, Z. Wang, Y. Tang, H. Bi, D. Wan and J. Lin, *Adv. Funct. Mater.*, 2013, **23**, 2263.
16 M. Zhou, H. Bi, T. Lin, X. Lü, D. Wan, F. Huang and J. Lin, *Carbon*, 2014, **75**, 314.
17 K. M. F. Shahil and A. A. Balandin, *Nano Lett.*, 2012, **12**, 861.
18 V. Goyal and A. A. Balandin, *Appl. Phys. Lett.*, 2012, **100**, 073113.
19 H. Malekpour, K. H. Chang, J. C. Chen, C. Y. Lu, D. L. Nika, K. S. Novoselov and A. A. Balandin, *Nano Lett.*, 2014, **14**, 5155.
20 J. D. Renteria, D. L. Nika and A. A. Balandin, *Appli. Sci.*, 2014, **4**, 525.
21 W. Cai, A. L. Moore, Y. Zhu, X. Li, S. Chen, L. Shi and R. S. Ruoff, *Nano lett.*, 2010, **10**, 1645.
22 S. Chen, Q. Wu, C. Mishra, J. Kang, H. Zhang, K. Cho, W. Cai, A. A. Balandin and R. S. Ruoff, *Nature mater.*, 2012, **11**, 203.
23 A. A. Balandin, S. Ghosh, W. Z. Bao, I. Calizo, D. Teweldebrhan, F. Miao and C. N. Lau, *Nano Lett.*, 2008, **8**, 902.
24 A. A. Balandin, *Nature Mater.*, 2011, **10**, 569.
25 D. L. Nika and A. A. Balandin, *J. Phys.: Condens. Matter.*, 2012, **24**, 233203.
26 Y. Zhu, S. Murali, M. D. Stoller, K. J. Ganesh, W. Cai, P. J. Ferreira, A. Pirkle, R. M. Wallace, K. A. Cychosz, M. Thommes, D. Su, E. A. Stach and R. S. Ruoff, *Science*, 2011, **332**, 1537.
27 J. Rafiee, X. Mi, H. Gullapalli, A. V. Thomas, F. Yavari, Y. Shi, P. M. Ajayan and N. A. Koratkar, *Nature Mater.*, 2012, **11**, 217.
28 A. C. Ferrari, J. C. Meyer, V. Scardaci, C. Casiraghi, M. Lazzeri, F. Mauri, S. Piscanec, D. Jiang, K. S. Novoselov, S. Roth and A. K. Geim, *Phys. Rev. Lett.*, 2006, **97**, 187401.
29 K. N. Kudin, B. Ozbas, H. C. Schniepp, R. K. Prud'homme, I. A. Aksay and R. Car, *Nano Lett.*, 2008, **8**, 36.
30 H. Bi, S. Sun, F. Huang, X. Xie and M. Jiang, *J. Mater. Chem.*, 2012, **22**, 411.
31 H. Bi, W. Zhao, S. Sun, H. Cui, T. Lin, F. Q. Huang, X. X. Xie and M. H. Jiang, *Carbon*, 2013, **61**, 116.
32 P. I. Ravikovitch and A. V. Neimark, *Langmuir*, 2002, **18**, 9830.
33 C. G. Liu, Z. N. Yu, D. Neff, A. Zhamu and B. Z. Jang, *Nano Lett.*, 2010, **10**, 4863.
34 C. Cui, W. Qian, Y. Yu, C. Kong, B. Yu, L. Xiang and F. Wei, *J. Am. Chem. Soc.*, 2014, **136**, 2256.
35 Y. W. Ma, J. Zhao, L. R. Zhang, Y. Zhao, Q. L. Fan, X. A. Li, Z. Hu and W. Huang, *Carbon*, 2011, **49**, 5292.
36 C. Chapotard and D. Tondeur, *Chem. Eng. Commun.*, 1983, **24**, 183.
37 L. L. Feng, J. Zheng, H. Z. Yang, Y. L. Guo, W. Li and X. G. Li, *Sol. Energy Mater. Sol. C*, 2011, **95**, 644.
38 A. Karaipekli, A. Sarı and K. Kaygusuz, *Renew. Energy*, 2007, **32**, 2201.
39 T. X. Li, J. H. Lee, R. Z. Wang and Y. T. Kang, Energy, 2013, 55, 752.
40 T. D. Dao and H. M. Jeong, *Sol. Energy Mater. Sol. C*, 2015, **137**, 227.
41 P. Goli, S. Legedza, A. Dhar, R. Salgado, J. Renteria and A. A. Balandin, *J. Power Sources*, 2014, **248**, 37.

Graphical Abstract

Carbon microtube/graphene hybrid structure has been prepared as a supporting framework to significantly improve thermal transport property of octadecanoic acid.